PNAS

Supplementary Information for

Tumor-polarized GPX3^{+} AT2 lung epithelial cells promote pre-metastatic niche formation

Zixin Wang[a,b], Jie Zhu[a], Yanfang Liu[a], Ziqiao Wang[c], Xuetao Cao[a,b,c], Yan Gu[a,1]

Corresponding: Yan Gu.

Email: guyan@immunol.org

This PDF file includes:

Figures S1 to S5

A

Cluster	Cell Type	Cell number of tumor sample	Percentage 1	Cell number of WT sample	Percentage 2	Tumor vs WT (P1/P2)
C0	AT2	1957	22.9%	3110	26.3%	0.87
C1	AT2	2076	24.3%	2347	19.9%	1.22
C2	AT2	923	10.8%	1847	15.6%	0.69
C3	AT2	788	9.2%	1604	13.6%	0.68
C4	AT2	270	3.2%	1005	8.5%	0.37
C5	Endothelial cell	853	10.0%	150	1.3%	7.85
C6	AT1	307	3.6%	626	5.3%	0.68
C7	AT2	607	7.1%	288	2.4%	2.91
C8	Ciliated cells	287	3.4%	415	3.5%	0.95
C9	Clara cells	334	3.9%	150	1.3%	3.07
C10	AT2	87	1.0%	243	2.1%	0.49
C11	Undefined	40	0.5%	12	0.1%	4.60
C12	Alveolar bipotent progenitor	21	0.2%	7	0.1%	4.14

B

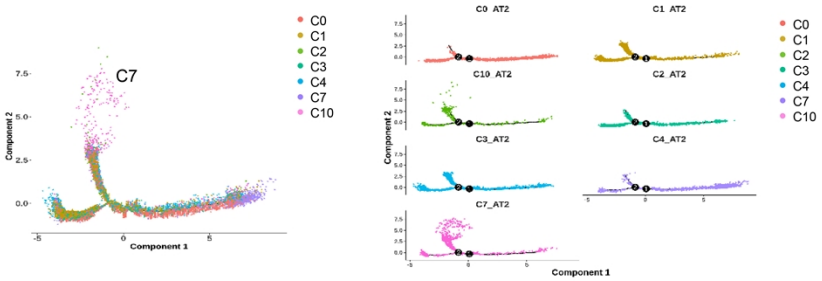

C

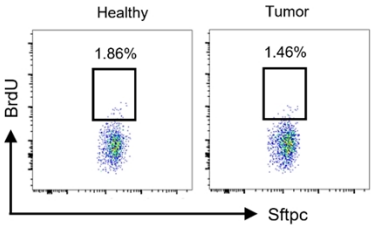

D

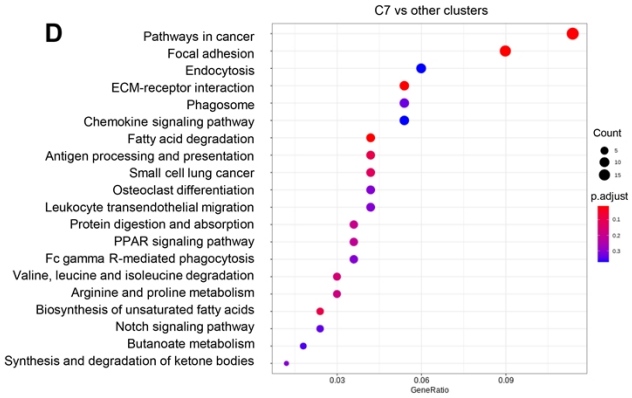

E

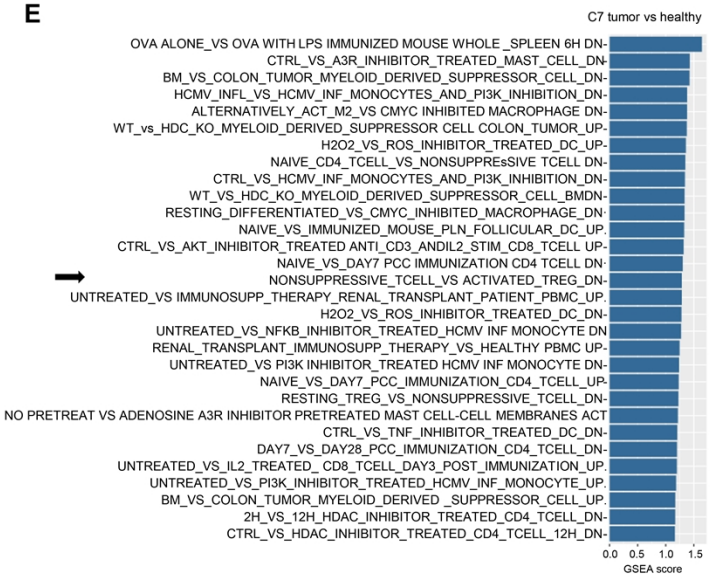

Fig. S1. Characteristics of cluster seven of AT2 cells. (A) Table of cell number and percentage of each cluster in lungs from LLC-bearing mouse and healthy one for scRNA-seq. (B) Pseudotime analysis of seven clusters in AT2 cells by Monocle 3. (C) Flow cytometry analysis of $Sftpc^{+}$ $BrdU^{+}$ AT2 cells in the lungs of tumor-bearing mice or healthy ones after 14-day feeding of BrdU. (D) KEGG analysis of related pathways of cluster seven cells verse other clusters from LLC tumor-bearing mice. (E) GSEA analysis of enriched pathways in cluster seven from LLC-bearing mouse vs healthy one from MSigDB (http://software.broadinstitute.org/gsea/msigdb).

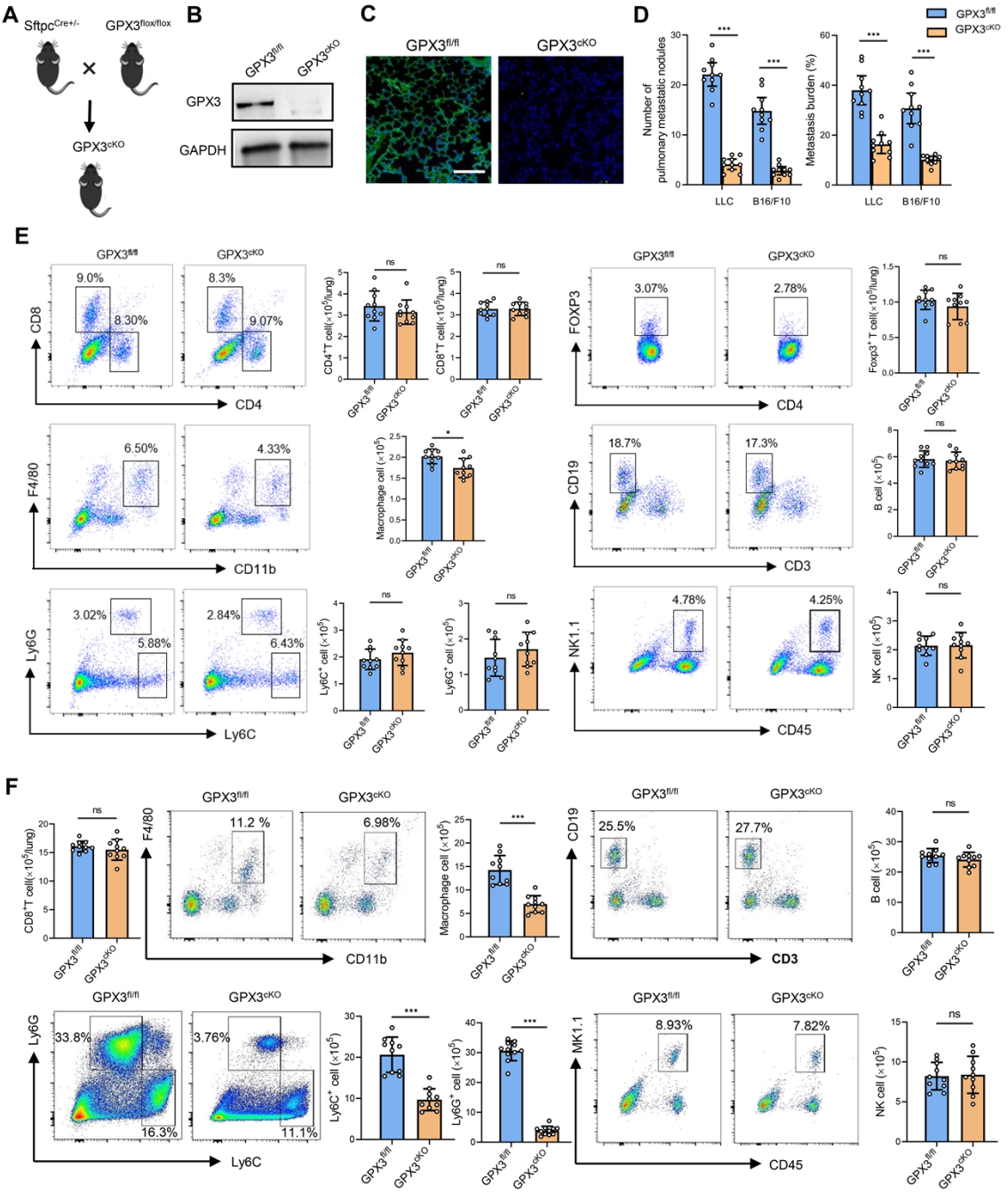

Fig. S2. Immune cell subpopulations in the lungs of the mice with conditional knockout of GPX3 in AT2 cells. (A) The schematic of experimental model of conditional knockout of GPX3 in AT2 cells by cross-breeding of $GPX3^{fl/fl}$ and AT2 cell-specific $Sftpc^{cre}$ mice. (B) Western blot analysis of GPX3 in the lung of $GPX3^{fl/fl}$ and $GPX3^{cKO}$ mice. GAPDH was used as a control. (C) Immunofluorescent analysis of GPX3 expression in the lung of $GPX3^{fl/fl}$ and $GPX3^{cKO}$ mice after LLC inoculation. Scale bar, 100 μm. (D) Quantitative analysis of pulmonary metastatic nodules and

metastasis burden of $GPX3^{fl/fl}$ or $GPX3^{cKO}$ mice. (E) Flow cytometric analysis of the proportions and absolute numbers of $CD4^+$ T, $CD8^+$ T cells, $CD4^+$ $Foxp3^+$ Treg cells, $CD11b^+$ $F4/80^+$ macrophages, $CD3^-$ $CD19^+$ B cells, $Ly6C^+$ $Ly6G^-$ monocytes, $Ly6C^{int}$ $Ly6G^+$ neutrophils and $CD45^+$ $NK1.1^+$ NK cells in the lung of $GPX3^{fl/fl}$ and $GPX3^{cKO}$ mice prior to tumor inoculation. (F) Flow cytometric analysis of proportions and absolute numbers of $CD11b^+$ $F4/80^+$ macrophages, $CD3^-$ $CD19^+$ B cells, $Ly6C^+$ $Ly6G^-$ monocytes, $Ly6C^{int}$ $Ly6G^+$ neutrophils and $CD45^+$ $NK1.1^+$ NK cells in the lung of $GPX3^{fl/fl}$ and $GPX3^{cKO}$ mice with LLC inoculation. Data are mean ± s.d. of one representative experiment. Similar results were seen in two independent experiments. Unpaired Student's t-tests, *, $P < 0.05$; ***, $P < 0.001$; ns, not significant.

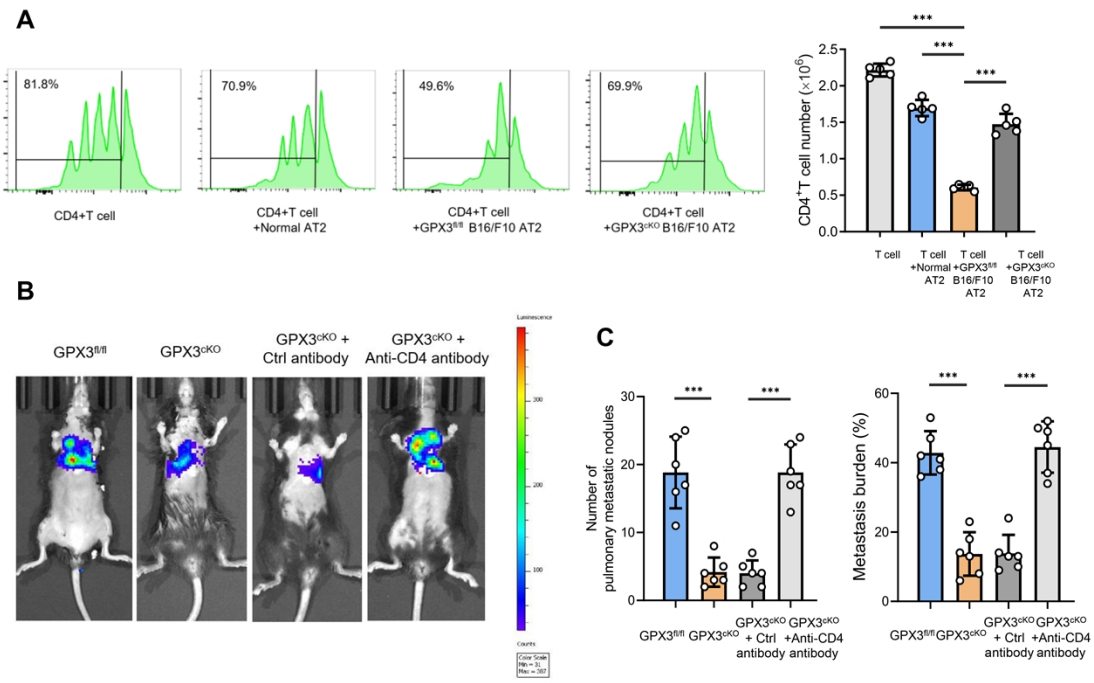

Fig. S3. Inhibition of T cell function and metastasis of AT2 cells is dependent on GPX3 and CD4⁺ T cells. (A) Representative images of CFSE-based proliferation assay and cell number of $CD4^+$ T cells when co-cultured with AT2 cells derived from healthy, B16/F10-bearing $GPX3^{fl/fl}$ or $GPX3^{cKO}$ mice respectively. (B and C) Representative images (B) and quantitative analysis (C) of lung metastasis of $GPX3^{fl/fl}$ or $GPX3^{cKO}$ mice with or without anti-CD4 antibody treatment detected by luciferase-based bioluminescence imaging (n=6) 40 days after LLC inoculation. Data are mean ± s.d. of one representative experiment. Similar results were seen in three independent experiments for A and in two independent experiments for B and C. Unpaired Student's t-tests, ***, P <0.001.

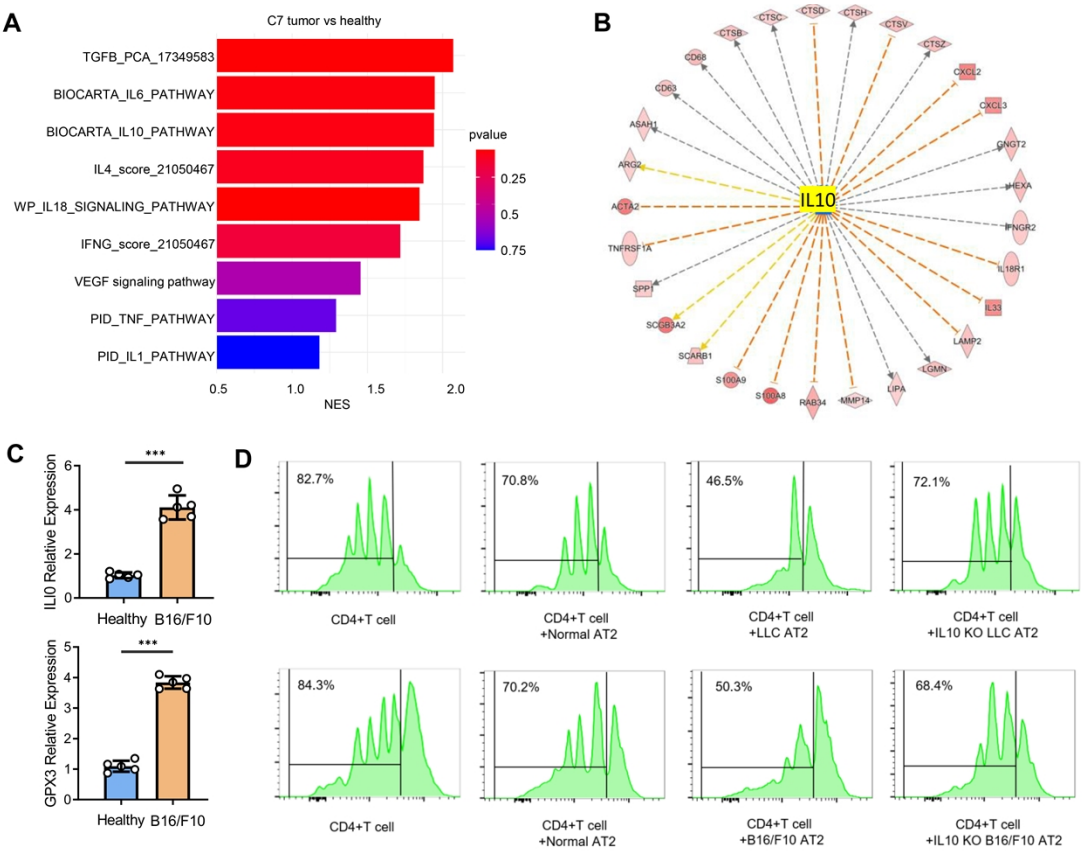

Fig. S4. IL-10 is required for the inhibition of T cell function by GPX3⁺ AT2 cells under tumor education. (A) GSEA analysis of related pathways of cluster seven cells from LLC-bearing mouse verse healthy one in single-cell data. (B) Ingenuity Pathway Analysis (IPA) analysis of interacted genes with IL10 of cluster seven cells from LLC-bearing mouse verse healthy one in single-cell data. (C) qPCR analysis of IL-10 and GPX3 expression in AT2 cells from tumor mice or healthy ones 14 days after B16/F10 inoculation. (D) Representative images of CFSE-based proliferation assay of $CD4^+$ T cells when co-cultured with AT2 cells derived from healthy, LLC- and B16/F10-bearing WT, or IL10 KO mice respectively. Data are mean ± s.d. of one representative experiment. Similar results were seen in three independent experiments. Unpaired Student's t-tests, ***, P <0.001. KO, knockout.

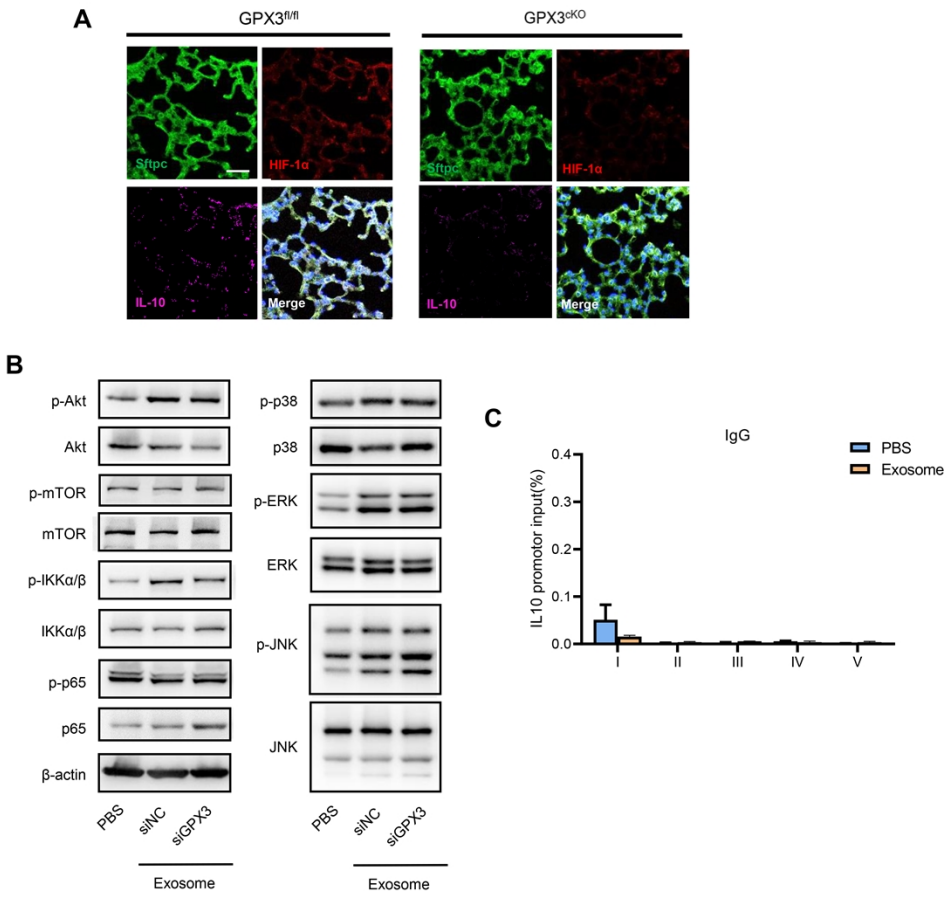

Fig. S5. Related signal pathways in tumor exosome-treated MLE-12 cells. (A) Immunofluorescent analysis of Sftpc, IL10 and HIF-1α expression in the lungs of $GPX3^{fl/fl}$ or $GPX3^{cKO}$ mice after LLC inoculation. Scale bar, 100 μm. (B) Protein level and phosphorylation of Akt, IKKα/β, mTOR, p65, p38, ERK and JNK in MLE-12 stimulated with tumoral exosomes were detected by Western blot. β-actin was used as control. (C) ChIP analysis of HIF-1α binding site with IL-10 promoter after tumor exosome administration. IgG was used as control.